MONITORING OF SPACE DEBRIS IN THE UV SPECTRAL RANGE

L.V. Granitsky, A.A. Cheremisin, V.A. Bartenev, and A.M. Il'inykh

Scientific Research Physical-Technical Institute,
Krasnoyarsk State University
Krasnoyarsk State Technical University
Scientific Production Association "Prikladnaya Mekhanika,"
Zheleznogorsk, Krasnoyarsk Region
Received December 3, 1997

The capabilities of the satellite UV systems to detect small bodies in the space near the Earth and in the upper atmosphere are discussed. The UV range from 200 to 300 nm *has the advantage, as compared to the IR and visible ranges, in the detection range for objects of a given size observed against the background of the Earth's surface illuminated by the Sun. This is caused by high contrast of the objects against the background in the UV due to the absorption of solar radiation by the upper-atmospheric ozone in the Hartley absorption band. One of the schemes developed for UV monitoring of the space debris is described.*

Monitoring of the near-Earth space is an urgent problem now. One aspect of this problem is the development of satellite systems for detecting of small bodies. Such systems can be applied to detection of "space debris"[1,2] and study of micrometeor fluxes and "mini-comets" comprising of ice.[3,4] The interest in studying the latter objects is stimulated by the fact they have been discovered only recently and by the hypothesis proposed in this connection on the extraterrestrial origin of the Earth's water envelope[3] and the atmospheric oxygen.[5] Timely remote detection of the dangerous heavenly bodies is also among the possible applications of such systems.[6]

Passive optical systems for the UV detection of small bodies from onboard a spacecraft have been developed at the Scientific Research Physical–Technical Institute at the Krasnoyarsk State University in cooperation with the Krasnoyarsk State Technical University.

The UV systems, as well as the systems operating in the IR and visible regions, can help to solve the problem of detecting sun-illuminated objects against the background of the space or the Earth at night. However, the UV spectral range has the advantage over the IR and visible ranges. This advantage consists in a wider detection range for an object of a given size observed against the background of the illuminated Earth's surface. This is caused by the high object-to-background contrast in the UV range from 200 to 300 nm due to the absorption of solar radiation by the atmospheric ozone in the Hartley absorption band.

Figure 1 shows the dependence of the spectral contrast coefficient K_λ on wavelength λ: $K_\lambda = (B_{\lambda o} - B_{\lambda b})/B_{\lambda b}$, where $B_{\lambda o}$ is the brightness of an object ideally scattering the solar radiation, and $B_{\lambda b}$ is the spectral brightness of the overall background of the Earth and the Earth's atmosphere illuminated by the Sun. The values of $B_{\lambda o}$ were calculated by the expression $B_{\lambda o} = \alpha E_\lambda / \pi$, where E_λ is the spectral density of solar radiation at the upper boundary of the Earth's atmosphere, α is the object's albedo (here it is assumed to be unity). The dependence[7] of E_λ on λ is also shown in Fig. 1. The marks on the curve indicate the percentage of the integral flux of the UV radiation with the wavelength shorter than the marked one in the total flux of the solar energy at the upper atmospheric boundary. To construct the K_λ curve, we used the data from Refs. 8–10. In the visible spectral range, the values of K_λ are about several units. The λ-dependence of K_λ obtained in the previous experiments proved to be close to the dependence shown in Fig. 1. (Our experiments in 1983–1986 have been conducted using the UV telescope of the space astrophysical station "Astron" operating in the range from 255 to 310 nm; the experiments of 1985–1987 have been carried out using the BUFS–1 spectrometer from onboard the "Meteor–3" satellite in the 280–340 nm range[11]; the data reported in Refs. 12 and 13 were obtained from "Nimbus–G"[12] in the range from 280 to 300 nm and "Nimbus–7"[13] in the range from 300 to 340 nm.)

As seen from Fig. 1, the maximum values of the contrast ($\sim 10^3$) are achieved in the wavelength range from 260 to 280 nm. Besides the high contrast one have to intercept the highest possible fraction of the light energy scattered by an object in order to enhance the detection range and to shorten the exposure time. This, in particular, leads to the requirement of a sufficiently wide operating wavelength range of the system. On this basis, we can determine the operating wavelength range to be from 200 to 300 nm. The average value of the

0235-6880/98/12 1142-05 $02.00

contrast coefficient K_λ calculated using the characteristics of the radiation flux integrated over the spectrum equals about 500 for this wavelength range.

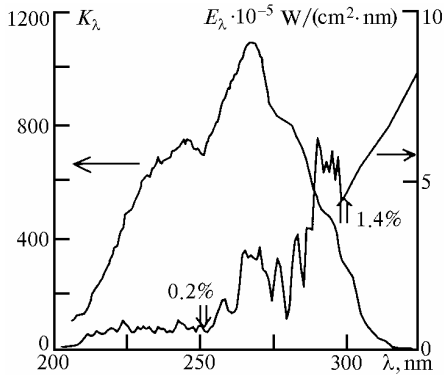

FIG. 1. The spectral coefficient K_λ of the object-to-background contrast in the UV spectral region. E_λ is the spectral density of the solar radiation flux at the upper atmospheric boundary.

The wavelength range chosen is characterized by a sufficiently high stability of the background level besides the high coefficient of spectral contrast. According to Ref. 13 for λ = 302 nm and the results of our experiments from onboard the "Astron" station for λ = 280 and 273 nm, random variations of the background spectral brightness are estimated as about 10-% rms deviations from the average value of the corresponding brightness.

The detection systems are characterized, first of all, by the maximum detection range for bodies of a given size. The maximum detection range L_{max} (all other factors being the same) determines the diameter of the effective entrance pupil D_{eff} and, thus, the aspect ratio of the entire system. Figure 2 shows the calculated results on L_{max} as a function of D_{eff} for bodies with some typical diameters: d_{eff} = 1 mm (collision with particles of this effective diameter d_{eff} becomes dangerous for spacecrafts[1]); 10 cm (it is the characteristic threshold diameter of objects detectable in the ground-based radar experiments[2]); d_{eff} = 10 m (the effective characteristic diameter of large space stations). The object's albedo of 0.4 value has been taken in calculation.

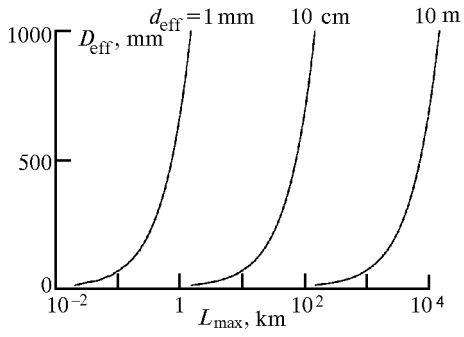

FIG. 2. The maximum detection range L_{max} for small objects detectable in the UV spectral range versus diameter of the entrance pupil D_{eff} of the detection system and the effective midsection diameter of an object d_{eff}.

The integral reflection coefficients for specimens of different materials have been studied at the Scientific Research Physical–Technical Institute of Krasnoyarsk State University. The value used is characteristic of the group of reflecting specimens. The characteristic values of the reflection coefficient for the group of slightly reflecting specimens are 3–7%.

The moon also has a low value of the albedo in the UV range (2–3%) (Ref. 10). The total density of the solar radiation flux in the UV range is $e_\sigma = 1.6 \cdot 10^{-3}$ W/cm^2, and the integral brightness is $b_\sigma = 10^{-6}$ W/cm^2·sr. The calculations have been made for an ideal detecting system: the spectral sensitivity of a matrix photodetector (MPD) was taken constant in the 200 to 300 nm range while zero outside this region. The D_{eff}/F_{eff} ratio of objective lens was taken 1/3.

The image of a point source on the MPD was assumed blurred due to defocusing. The size of a defocusing spot was taken to be 2 by 2 pixels. This value is a compromise between the requirement of extending the detection range and accurate determination of coordinates of a sufficiently bright object. As calculations show, to meet the latter requirement, the size of the defocusing spot should equal from 4 by 4 to 9 by 9 pixels. The linear dimension of a pixel equals 20 μm. The detection criterion assumes a 40% enhancement of the signal from image recording cells over the background level. This criterion corresponds to the detection mode at a sufficiently long exposure time τ such that the main factor governing the probability of false detection ($p_{fd} \sim 0.01$) are the fluctuations of the background noise. The fluctuations are being estimated by a Gaussian distribution with a 10-% standard deviation. As seen from Fig. 2, the systems incorporating a telescope with a relatively small diameter D_{eff} = 200 mm and relatively large D/F ratio (D_{eff}/F_{eff} = 1/3) allow detection of small bodies at rather far distances.

When small bodies are observed near an edge of the illuminated part of the Earth's disk, the detection really comes against the background due to parasitic stray light. The level of this stray light background can only be reduced down to some level that is actually determined by the level of technology used. The level of this technological background light noise can be presented as the effective brightness, which makes up certain fraction of the actual source brightness. For good objective lenses this part is less than 1%. According to our studies, for the UV telescope of the "Astron" station it comprises about 0.4% (Ref. 14). Under these conditions, the object-to-background contrast is high enough ($\geq 10^2$) in the visible and in the UV spectral regions. However, the background in the UV is several orders of magnitude lower than in the visible. According to estimates made, systems operating in the UV spectral range can provide for the maximum detection range, which is an order of magnitude larger than the maximum detection range with the systems operating in the visible region. Thus, the UV range holds its advantage in the maximum detection

range when observing small bodies near the edge of the illuminated part of the Earth's disk.

Figure 3 presents a generalized block-diagram of a UV detection system under development intended for detection of small bodies. The system includes two telescopes with the schemes also presented in Fig. 3. Pictures of the telescopes are shown in Fig. 4.

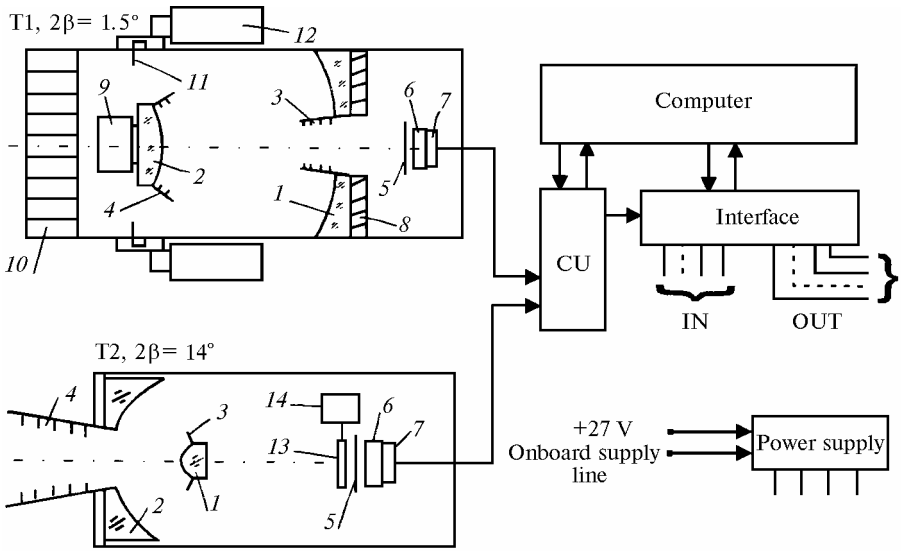

FIG. 3. The generalized block-diagram of the detection system and optical arrangement of its telescopes: the Ricci–Kretien telescope (T1); the Bowen telescope (T2); the secondary voltage converters (Power supply); the electronic unit for control over the instruments and signal converters of the CCD matrix; the interface to the onboard telemetry (Interface); the onboard computer (Computer); input and output to the spacecraft telemetry (IN and OUT); the primary mirror (1); the secondary mirror (2); the blind of the primary mirror (3); the blind of the secondary mirror (4); the additional cutoff filter (5); the matrix photoreceiver (CCD matrix) (6); the Peltier cooler of the CCD matrix (7); the primary mirror holder (8); the focusing and fastening unit of the secondary mirror (9); the cellular blind (10); the iris shutter (11); the iris shutter drive (12); the shutter (13); the shutter drive (14).

The wide-angle Bowen telescope serves for recording general visual situation, and for rough guiding using bright stars. The narrow-angle Ricci–Kretien telescope serves for a detailed study of the space domain analyzed. The main parameters of the Ricci–Kretien telescope are the following: field of view is 1.5°, diameter of the primary mirror is 200 mm, diameter of the secondary mirror is 75 mm, equivalent focal length is 1200 mm, resolution (over the matrix) is 10 arc sec., diffraction resolution: 1.3 arc sec. at the field center and 3.8 arc sec. on the field edge, mass (with the electronic equipment) is 12 kg, overall dimensions – ∅250 × 800 mm, power consumption is 15 W. The Bowen telescope has the following parameters: field of view is 14°, primary mirror diameter is 60 mm, secondary mirror diameter is 150 mm, equivalent focal length is 115 mm, mass is 12 kg, overall dimensions are ∅200 × 520 mm. The mirrors of both telescopes are coated with $Al + MgF_2$.

The sensitivity of the MPD used is maximum at the wavelength about 280 nm. Additional filters, which cut off radiation with the wavelength above 300 nm, are set in front of the MPD. The CCD matrix generates the video signal.

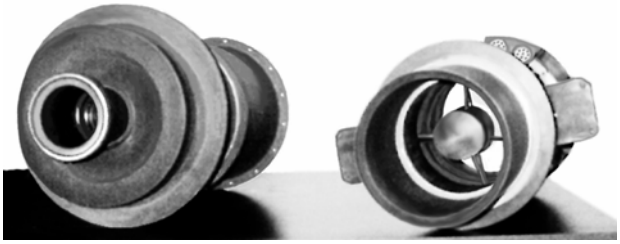

FIG. 4. The telescopes of the system intended for detection of small bodies: the Bowen telescope (left) and the Ricci-Kretien telescope (right).

The choice of the CCD matrix as a video signal generator provides for:

– the wide dynamic range (up to several thousands);

– strict raster, insensitive to variations of supply voltage, temperature, and magnetic fields, what provides high accuracy of the object's coordinate measurements;

– low power consumption, high reliability, small size and mass.

The system has been designed to be operated with the CCD matrices of 512 by 512 and 1024 by 1024 elements. To reduce the internal noise and smooth the inhomogeneities of the dark current, the CCD matrix is cooled down to −40 ... −60°q with a thermoelectric Peltier microcooler. This temperature is stabilized to provide for stability of the CCD matrix parameters. Thermal stabilization allows significant (up to two orders of magnitude) increase in the sensitivity of the CCD matrix.

The secondary voltage converter (see Fig. 3) serves as a power supply for all the system's units from the onboard supply line and for galvanic decoupling of circuits when necessary.

The operation of the instrument is controlled by the onboard computer. Toward this end, all system's units are connected to the computer by the inter-unit interface trunk. The system programs, that is, the program of the initial start, the information exchange programs, the programs of input and output to the telemetry, the program of information exchange with other units, the programs of response to technological signals and emergency situations, as well as constants, star catalogues, etc., are stored in the computer ROM. Running programs, intermediate results, and foreground information from other units are in the computer RAM.

The main function of the control unit is to form video signals from the CCD matrix and to monitor their parameters. Video signals from the CCD matrix are amplified, and noise of the CCD phase switching is suppressed. The schemes of control over the CCD matrix allows changing of the video signal storage parameters and the sweep parameters. Other functions of the control unit include control over the microcooler of the CCD matrix, temperature monitoring, control over the iris shutter drive and some other instrument's transducers.

The interface of the onboard systems is responsible for receiving signals coming from the telemetry and transforming them into the computer commands.

The scheme of image processing for detection of a sun-illuminated object against the background of the Earth's surface both illuminated by the Sun and dark includes the following stages. A pulse from a point object is separated out from the background noise having a multiplicative component caused by variable sensitivity of the CCD-matrix cells, including possible defects in some cells and defects of rows and columns. Besides, there are dark noise and noise caused by the quantum fluctuations of a signal.

To decrease the noise level, image filtration and signal intensity leveling by the sensitivity of different MPD elements are used. In the case of maximum detection ranges, a small excess of a signal from a group of CCD-matrix cells over the signal level from the cells that measure background radiation serves as the detectability criterion. In this case, it is expected that for the exposure time longer than 1 ms the main contribution into the total noise and the probability of false detection comes from variations in the background brightness of the sun-illuminated Earth's surface.

The algorithm for detection of objects against the background of the space also provides for excluding the reference stars falling within a frame from the list of pulses. These stars are selected from the star catalogue.

At this stage of the development, image frames or their fragments are transmitted for further processing on the Earth. This is needed to improve the processing technique. As seen from the Table I of the information flow parameters, the problem of object detection is connected with processing of bulky information.

TABLE I.

Matrix dimensionality	The number of matrix elements	Bit	Frame, MBit	Transmission time for one frame**, s	The number of frames transmitted in one session ***
512 × 512	$2.62 \cdot 10^5$	8+2*	2.5	26	23
1024 × 1024	$1.04 \cdot 10^6$	8+2*	10	103	5

*Service bits.
**At the telemetry carrying capacity of 100 KBit/s.
***For a communication session 10 min. long.

At the next stage of the development, the matrix images will be processed autonomously onboard a spacecraft under the control of a specialized video processor.

REFERENCES

1. V.L. Ivanov, V.A. Men'shikov, L.A. Pchelintsev, and V.V. Lebedev, *Space Debris* (Patriot, Moscow, 1996), Vol. 1, 360 pp.
2. L.S. Novikov, N.N. Petrov, and Yu.A. Romanovskii, *Ecological Aspects of Astronautics* (Znanie, Moscow, 1986), Issue 5, 64 pp.
3. L.A. Frank, L.B. Sigwarth, and J.D. Craven, Geophys. Res. Lett. **13**, No. 4, 307–310 (1986).
4. C.M. Yeates, Planet. Space Sci. **37**, No. 10, 1185–1196 (1989).
5. V.N. Lebedinets, Astronomicheskii Vestnik **25**, No. 3, 350–363 (1991).
6. *Problems of Earth Protection against Collision with Dangerous Space Objects (SPE-94), Abstracts of Reports at the International Conference*, Snezhinsk (Chelyabinsk-70) (1994): Vol. I, 113 pp.; Vol. II, 140 pp.
7. O. Wait, ed., *Solar Energy Flux and Its Changes* [Russian translation] (Mir, Moscow, 1980), 600 pp.
8. V.A. Krasnopol'skii, A.P. Kuznetsov, and A.I. Lebedinskii, Geomagnetism i Aeronomiya **6**, No. 2, 185–189 (1966).
9. R.E. Huffman, F.J. Le Blance, J.C. Larrebee, and D.E. Paulsen, J. Geophys. Res. **85**, No. A5, 2201–2215 (1980).

10. V.B. Vasil'ev, T.M. Grechko, et al., *Optical Studies of the Atmospheric Radiation, Aurora Borealis, and Noctilucent Clouds from Onboard the Orbital Scientific Station "Salyut-4"* (Publishing House of the Institute of the Astronomy and Atmospheric Physics, ESSR Academy of Sciences, Tallin, 1977), 178 pp.
11. D.A. Andrienko, V.I. Barysheva, et al., Issled. Zemli iz Kosmosa, No. 1, 67–73 (1990).
12. D.P. Heath, F.J. Krugger, H.A. Roeder, and B.D. Henderson, Opt. Eng. **14**, No. 4, 323–331 (1975).
13. J.E. Frederick and G.N. Serafino, Tellus **B39**, No. 3, 261–270 (1987).
14. Cheremisin, L.V. Granitskii, V.M. Myasnikov, N.V. Vetchinkin, and V.V. Slabko, Atmos. Oceanic Optics **11**, No. 8, 744–748 (1998).